Fuel 112 (2013) 263–271

Contents lists available at SciVerse ScienceDirect

Fuel

journal homepage: www.elsevier.com/locate/fuel

Measurements of laminar flame speeds and flame instability analysis of 2-methyl-1-butanol–air mixtures

Qianqian Li, Erjiang Hu *, Yu Cheng, Zuohua Huang *

State Key Laboratory of Multiphase Flow in Power Engineering, Xi'an Jiaotong University, Xi'an 710049, People's Republic of China

HIGHLIGHTS

- Laminar flame speeds of 2MB–air mixture were measured.
- Comparison on laminar flame speeds of various fuels was made.
- Flame instabilities were analyzed combining with schlieren photos.
- Correlation of laminar flame speeds is provided.

ARTICLE INFO

Article history:
Received 1 February 2013
Received in revised form 12 March 2013
Accepted 11 May 2013
Available online 28 May 2013

Keywords:
2-Methyl-1-butanol
Laminar flame speed
Flame instability
Comparison

ABSTRACT

Laminar flame speeds of 2-methyl-1-butanol (2MB)–air mixture at temperatures of 393, 433 and 473 K, pressures of 0.1, 0.25, 0.5 and 0.75 MPa, and equivalence ratios of 0.6–1.8 were measured using the spherically propagating flame. Flame instabilities were analyzed using the Lewis number, flame thickness, density ratio and Markstein length combining with the schlieren photos. Flame instability is insensitive to temperature while it increases with the increase of pressure. A correlation of laminar flame speed is provided on the basis of experimental data. Comparison was made between the laminar flame speeds of 2-methyl-1-butanol and ethanol, n-butanol and iso-octane. Results show that 2-methyl-1-butanol has the close values of laminar flame speed with those of n-butanol, but lower than those of ethanol and higher than those of iso-octane.

1. Introduction

With increasing concerns on energy demand and environmental protection, the studies and utilization of biofuels have been attracting more and more attention. Biofuels can be produced from the living organisms, biomass conversion and various biogases [1]. Bio-alcohols, is produced in fermentation of sugars, starches and cellulose through the action of microorganisms and enzymes. As a first generation biofuel, ethanol has been used as the fuel additive to gasoline. Since the existence of some disadvantages of ethanol, such as high hygroscopicity, low heating value and corrosivity, the concerns for the large alcohols like bio-butanol are increasing. Butanol has higher energy density and better solubility with gasoline. It can be directly used in engine without any changes in engine structure [2–5].

Table 1 shows the physical characteristics of different fuels. 2-Methyl-1-butanol (2MB) is one of pentanol isomers. Comparing with ethanol and n-butanol, 2MB has the advantages of high heating value, low hygroscopicity, low vaporization pressure and better solubility with gasoline [6].

Recently, researches were conducted on the production of 2-methyl-1-butanol. In fact, 2-methyl-1-butanol is natural by-product of microbial fermentations from amino acid substrates, but the amount is small and cannot meet the application requirement [7]. Recently, Cann et al. [8,9] developed an approach to increase the production of 2-methyl-1-butanol in engineered Escherichia coli. Progress was reported on the photosynthetic production of 2-methyl-1-butanol from CO_2, which is favorable to the lowering of atmospheric CO_2 [10]. As the biologically engineered pentanol production demonstrates a good prospect, thus the utilization of 2-methyl-1-butanol in power equipments will become a reality. Fundamental study of this fuel can understand the combustion characteristics and provide the basic information for fuel chemical kinetics development.

Laminar flame speed is a key parameter of fuel and is the base to determine the turbulent flame speed. Laminar flame speed can be used to validate and develop the fuel chemical kinetics. Laminar flame speeds of alcohol fuels were measured in the past decade. Metghalchi et al. [11] and Saeed et al. [12] measured the laminar

* Corresponding authors. Tel.: +86 29 82665075; fax: +86 29 82668789 (Z. Huang).
E-mail addresses: hu2jiang@163.com (E. Hu), zhhuang@mail.xjtu.edu.cn (Z. Huang).

0016-2361/$ - see front matter © 2013 Elsevier Ltd. All rights reserved.
http://dx.doi.org/10.1016/j.fuel.2013.05.039

Table 1
Physical properties of fuels.

	Ethanol	N-butanol	Isooctane	2MB
Oxygen content (mass%)	0.35	0.22	0	0.18
Density (kg/m^3)	789	810	692	815.2
Energy–volume density (kJ/cm^3)	21.11	26.9	31.87	28.38
Octane number (R + M)/2	100	87	95–96	–
Lower heating value (MJ/kg)	28.9	33.1	44.3	34.65
Vapor pressure at 21 °C (kPa)	5.95	0.56	5.5	0.4
Flash point (°C)	13–14	35	−12	50
Self ignition temperature (°C)	363	343	396	385
Boiling temperature (°C)	78.37	118	99.3	128.7
Melting point (°C)	−114	−90	−107.4	−70
Solubility in water at 20 °C (g/l)	Unlimited immiscible	63.2	0.002	31

flame speeds of methanol using a constant volume bomb without considering the flame stretch effect on flame front. Liao et al. [13] and Zhang et al. [14] measured the laminar flame speeds of methanol at various temperatures and pressures. Laminar flame speeds of ethanol were measured by Gulder [15], Liao et al. [16] and Marinov et al. [17]. Broustail et al. [18] measured the laminar flame speeds of ethanol and butanol. Their results showed that both ethanol and butanol have the faster laminar flame speed than that of iso-octane. Veloo et al. [19] measured the laminar flame speeds of four butanol isomers using the counter-flow flame at atmospheric pressure and temperature of 343 K. Gu et al. [20] measured the laminar flame speeds of four butanol isomers using the spherically propagating flame at different initial temperatures and pressures.

Up to now, reports on combustion of 2-methyl-1-butanol is very limited. The reported work mainly concentrated on the n-pentanol and 3-methyl-1-butanol [21–24]. Zhao et al. [6] reported the thermal decomposition of pentanol isomers, including the 2-methyl-1-butanol. Recently, Tang et al. [25] proposed a kinetic mechanism for the 2-methyl-1-butanol on the basis of measured ignition delay times, but their mechanism has not been validated by the laminar flame speed. Thus, providing the laminar flame speeds of 2-methyl-1-butanol is required.

In this study, the laminar flame speeds of 2-methyl-1-butanol at three temperatures (393 K, 433 K, 473 K), four pressures (0.1 MPa, 0.25 MPa, 0.5 MPa, 0.75 MPa), and equivalence ratios from 0.6 to 1.8 were measured using the spherically propagating flame. Flame instabilities at different temperatures, pressures and equivalence ratios were analyzed. A correlation to calculate the laminar flame speeds of 2-methyl-1-butanol was given on the basis of experimental data. Comparisons on laminar flame speeds of ethanol, n-butanol and 2-methyl-1-butanol were provided.

2. Experimental setup and data processing

2.1. Experimental setup

The experimental setup was described in details in previous literatures [26–29]. Here, only a brief description is given. It includes a constant volume combustion chamber, the heating system, the ignition circuit, the data acquisition, and the high-speed schlieren photography. The combustion chamber is of a cylinder type with an inner diameter of 180 mm and volume of 5.5 L. The centrally located electrodes are used to ignite the combustible mixture. The pressure transmitter, thermocouple, pressure transducer, liquid fuel injection valve, and inlet and outlet valves are mounted on the chamber body. Two quartz windows of 80 mm diameter are mounted on the two sides of the vessel. A high-speed digital camera (HG-100K) operating at 10,000 frames per second recorded the flame progression during the combustion. The partial pressures of each component are regulated by a mercury manometer when the initial pressure of the mixtures in the vessel is less than or equal to 0.1 MPa, and the partial pressures are regulated by the pressure transmitter at initial pressures greater than 0.1 MPa. The entire vessel was heated by a 2.4 kW heating-tape wrapped outside the chamber body. The thermocouple measures the initial temperature of mixtures in the vessel with an accuracy of 1 K. The initial temperature is adjusted by a thermo-regulator. When the mixture reaches the designated initial temperature, the power is switched off. The required liquid fuel is injected into the chamber by the microliter syringes corresponding to the given initial temperature, initial pressure, and equivalence ratio. Bomb dry air is supplied into the chamber through the inlet/outlet valve. A wait of 8–10 min is allowed before the ignition starts.

2.2. Data processing

The stretched flame speed is determined by

$$S_b = \frac{dr_f}{dt} \tag{1}$$

where the unstretched flame speed, S_b^0, is the flame speed at zero stretch rate. There exists a linear relationship between the stretch flame speed and unstretched flame speed,

$$S_b^0 - S_b = L_b\kappa \tag{2}$$

where L_b is Markstein length of the unburned mixture. Through the continuity across the flame front, laminar flame speed is calculated using the equation

$$S_u^0 = \rho_b^0 S_b^0/\rho_u \tag{3}$$

where ρ_u and ρ_b^0 are the unburned gas density and burned gas density, respectively. The adiabatic temperature, T_{ad}, can be calculated through thermal equilibrium theory. The flame thickness is defined as

$$l_f = \nu/S_u^0 \tag{4}$$

Simulations on laminar flame speeds of ethanol, n-butanol and iso-octane were made with the Chemkin Premix code with detailed chemistry and transport. Marinov's mechanism [17] is used to calculate the laminar flame speeds of ethanol while Sarathy's mechanism [30] is used to simulate the laminar flame speeds of n-butanol.

3. Results and discussions

3.1. System validation

The experimental apparatus in this study have been used to measure the laminar flame speeds of many fuels and over a large temperature and pressure range [27,28,31]. To further prove the

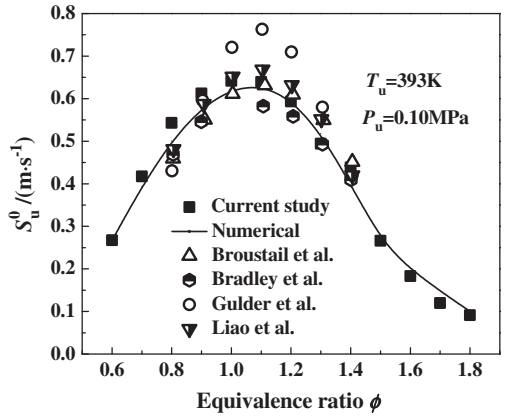

Fig. 1. Laminar flame speeds of ethanol at P_u = 0.1 MPa, T_u = 393 K.

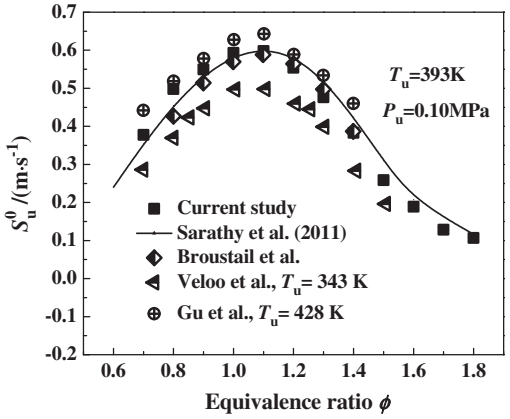

Fig. 2. Laminar flame speeds of n-butanol at P_u = 0.1 MPa.

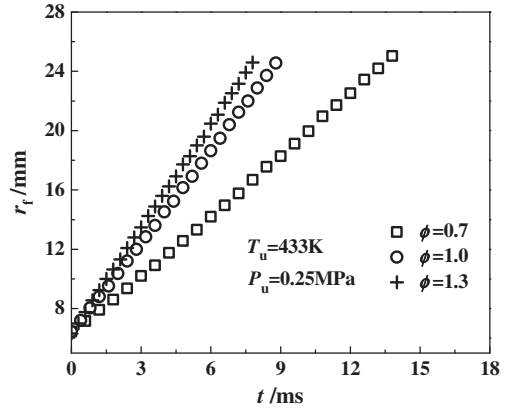

Fig. 3. Flame radius versus time.

accuracy of the system, additional measurements on ethanol and n-butanol were conducted and simulations were made with the very recently developed mechanisms.

Fig. 1 shows the comparison the measured laminar flame speed of ethanol–air mixtures with those of previous studies [15,16,18,32]. All the data were measured with the spherically propagating flame at T_u = 393 K and P_u = 0.1 MPa. All data are in good agreement except the literature [15]. This study provides the values at extended equivalence ratios. Simulations using the Marinov's mechanism [17] give good predictions on the laminar flame speeds of ethanol.

Fig. 2 gives the comparison of the measured laminar flame speeds of butanol with those of literatures [32] [19,33]. The measured values (at 393 K) have good agreement with those of Broustail et al. [18]. Simulations using the Sarathy's mechanism [30] give good prediction on the measured laminar flame speeds. The values of Gu et al. [33] is higher than the measured values due to its higher initial temperature and those of Veloo et al. [19] is lower than the measured values due to its lower initial temperature. Anyway, the comparison between the experimental results and the simulations both focuses on the ethanol and butanol, and it gives the high accuracy in measuring the laminar flame speed with this experimental setup.

3.2. Laminar flame speed

In this study, flame radius between 6 mm and 25 mm was used to determine the laminar flame speed and Markstein length to remove the effect of spark ignition, pressure rise and system confinement [34,35,32]. Fig. 3 shows the flame radius versus time at three equivalence ratios. Flame radius increases almost linearly with the increase of time. The stoichiometric mixture propagates faster than both lean and rich mixtures.

Fig. 4 gives the stretched flame speed versus stretched rate at different temperatures and pressures. The stretched flame speed decreases linearly with the increase of stretch rate. The slope of stretched flame speed versus stretched rate is the negative value of Markstein length. Markstein length, L_b, reflects the effect of stretch on flame and is the characteristic parameter of flame instability. Large value of Markstein length corresponds to stable flame

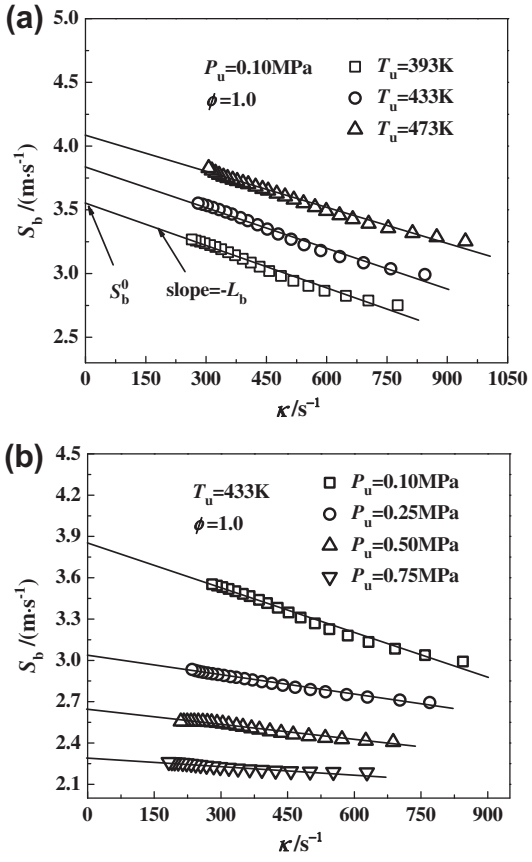

Fig. 4. Stretched flame speed versus stretched rate.

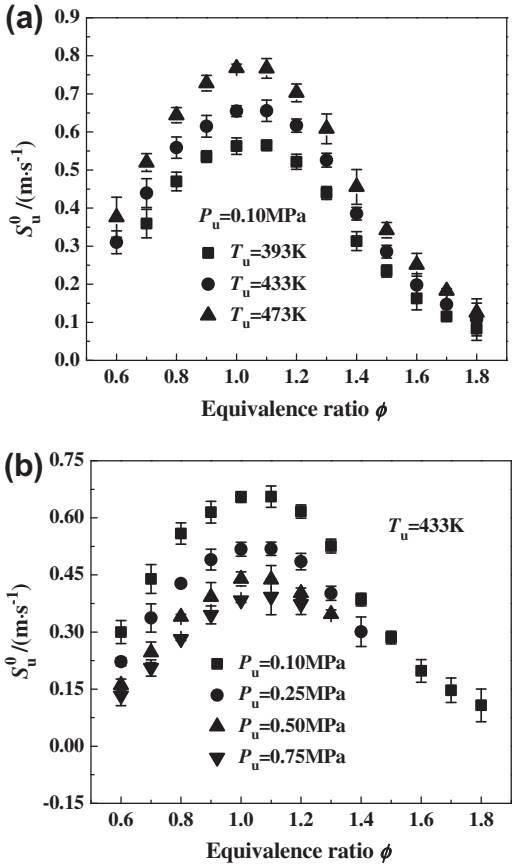

Fig. 5. Laminar flame speeds versus equivalence ratio at different temperatures and pressures.

front. Fig. 4a shows that the stretched flame speed increases with the increase of temperature. The slope of stretched flame speed versus stretch rate does not change with the increase of temperature which suggests little effect on flame front instability with the variation of temperature. As shown in Fig. 4b, the stretched flame speed decreases with the increase of pressure. The slope of stretched flame speed versus stretch rate is increased with the increase of pressure, and this indicates the increase of flame front instability as pressure is increased.

When flame radius is infinite, the stretch rate will become zero, thus, the unstretched flame speed can be determined, as shown in Fig. 4, when extrapolating the line to the zero stretch rate. Laminar flame speed is determined on the basis of conservation of mass on flame front. Fig. 5 gives the laminar flame speeds of 2-methyl-1-butanol versus equivalence ratio at different temperatures and pressures. Laminar flame speed increases with increasing the temperature and decreasing the pressure. Laminar flame speeds give their peak values at the equivalence ratios between 1.0 and 1.1.

Adiabatic flame temperature, T_{ad}, and mass burning flux ($f = \rho_u S_u^0$) are key parameters of the laminar premixed flame. Mass burning flux is a comprehensive index reflecting the information of exothermicity, reactivity and diffusivity [36]. It is the product of unburned mixture and laminar flame speed. Fig. 6 gives the adiabatic flame temperature and mass burning flux at three elevated temperatures and four pressures. Mass burning flux gives the consistent trend to that of adiabatic flame temperature versus the equivalence ratio. Both give their peak values at the equivalence ratio between 1.0 and 1.1. They increase with increasing temperature and pressure. The results reveals that the increasing effect on laminar flame speed is higher than decreasing effect on density of the unburned gas as temperature is increased. However, the decreasing effect on laminar flame speed cannot cover the substantial increase of the density of unburned mixture as pressure is increased. With the increase of pressure, the increasing effectiveness is increased for mass burning rate and is little for adiabatic flame temperature. This behavior tends to be more significant at stoichiometric ratio.

Laminar flame speed can be correlated in the form of

$$S_u^0 = UP_u^{\varepsilon_p} \tag{5}$$

where P_u is initial pressure, U and ε_p are the fitting constants. Fig. 7 gives the fitting curves of laminar flame speeds versus pressure at lean, rich and stoichiometric mixtures. Laminar flame speed decreases exponentially with the increase of pressure. This has been reported in the previous studies on methane, iso-octane, dimethyl ether [32,37,38]. Laminar flame speed and pressure has the relationship of $S_u^0\tilde{\omega}^{1/2}/\rho_u\tilde{p}^{(-1+n/2)}$. The reaction order, n, calculated by equation $n = 2(\varepsilon_p + 1)$ [31,36] is shown in Fig. 8. Reaction order is increased with the increase of equivalence ratio at lean mixture side, and is insensitive to the variation of equivalence ratio from stoichiometric mixture to rich mixture. Reaction order gives the values between unit and two. Reaction order depends on the contributions from both branching chain reaction and chain termination reaction. Sensitive analysis at elevated temperature on alcohol fuel showed the enhancement of chain branching reaction and little effect on chain termination reaction [39]. For the lean mixture, the adiabatic flame temperature increases with the increase of equivalence ratio, as shown in Fig. 6, leading to the increase of the reaction order. Similar phenomenon was reported in previous literature [40].

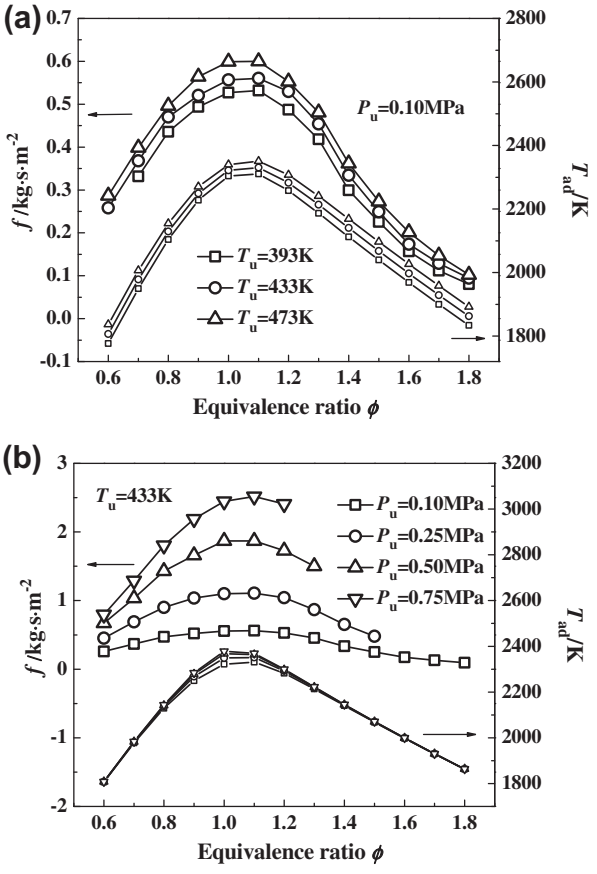

Fig. 6. Mass burning flux and adiabatic flame temperature versus equivalence ratio.

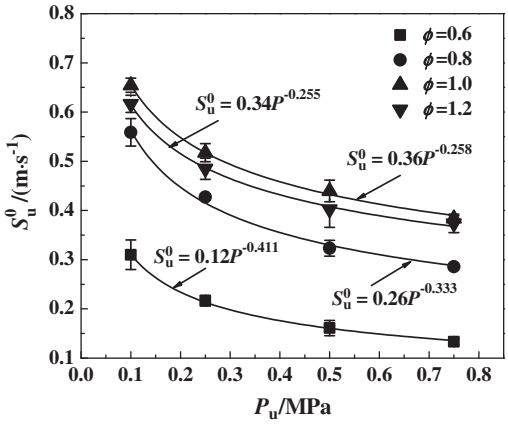

Fig. 7. Laminar flame speed versus pressure at different equivalence ratios.

3.3. Flame instability

For the spherically expanding flame, there exist three types of instability, the diffusional–thermal instability, the hydrodynamic instability and the buoyancy instability. As buoyancy instability appears in the flames with very slow propagation speed, such as lean limit mixture and/or rich limit mixture, which are not the mixtures in this study, thus only the diffusional–thermal instability, the hydrodynamic instability are considered in the following analysis. Diffusional–thermal instability is characterized by the Lewis number, *Le*, which is defined as the ratio of mixture thermal to mass diffusivity [36,41]. The hydrodynamic instability, caused by the density jump across the flame front, is enhanced at high density jump [42,43]. Hydrodynamic instability will dramatically affect the flame front pattern at the elevated pressure. Markstein length has the relationship with Lewis number as,

$$L_b = l_f\left[\sigma^{-1}\gamma_1 + \frac{1}{2}Ze(Le-1)\gamma_2\right] \quad (6)$$

where $\gamma_1 = \frac{2\sigma}{(1+\sqrt{\sigma})}$, $\gamma_2 = \left(\frac{4}{\sigma-1}\right)\{\sqrt{\sigma} - 1 - \ln[0.5(\sqrt{\sigma}+1)]\}$ [44]; and Ze is Zeldovich number, which can be expressed as $Ze = E_a(T_a - T_u)/R(T_a)^2$, where E_a is activation energy and R is universal gas constant; *Le* is effective Lewis number of the mixture. Markstein length reflects the overall behavior of flame instability.

Fig. 9 gives the Lewis number and Markstein length versus equivalence ratio at elevated temperatures and pressures. The density ratio and flame thickness versus equivalence ratio at elevated

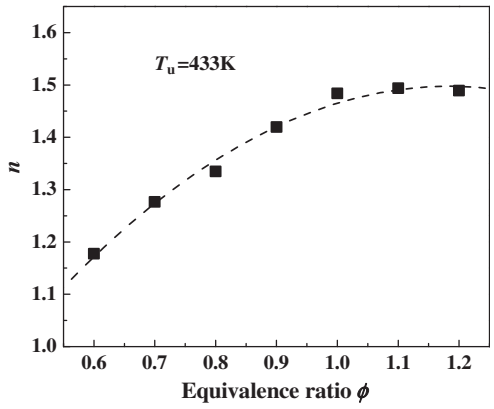

Fig. 8. Reaction order versus equivalence ratio.

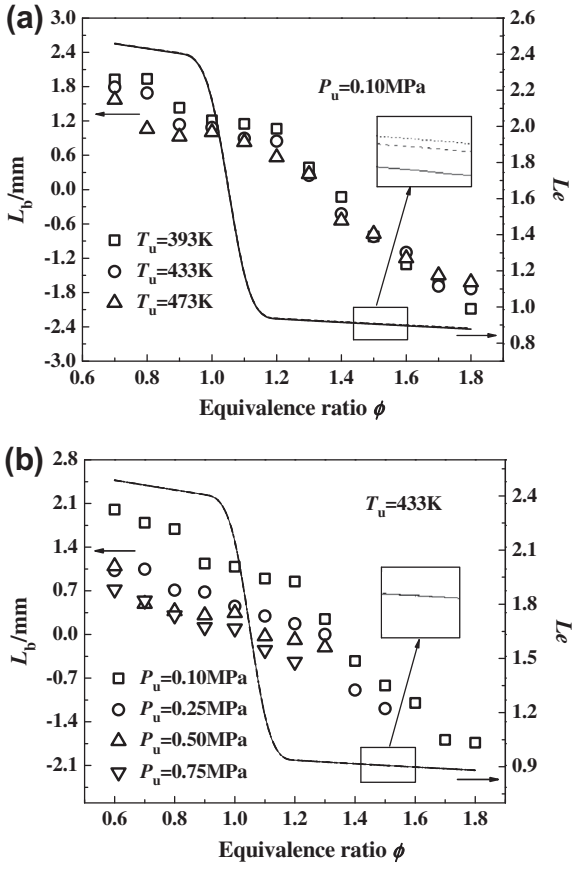

Fig. 9. Markstein length and Lewis number versus equivalence ratio. (a) Solid line: 393 K, dash line: 433 K, short dash line: 473 K; and (b) solid line: 0.1 MPa, dash line: 0.25 MPa, dot line: 0.5 MPa, dash dot line: 0.75 MPa.

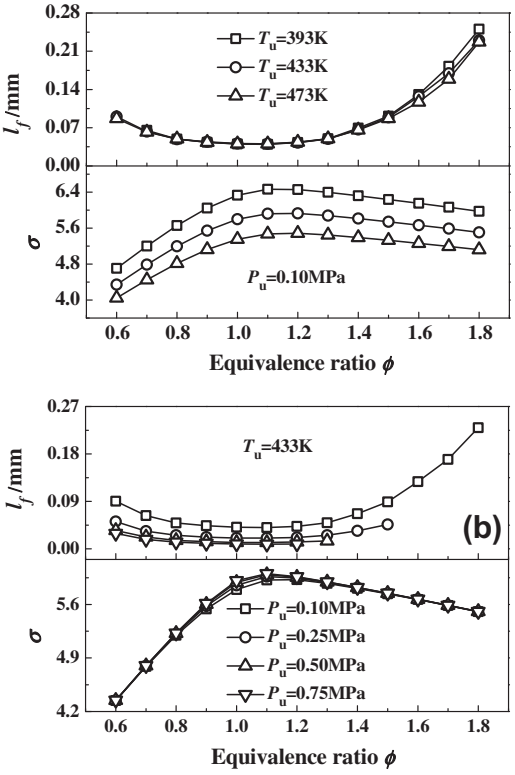

Fig. 10. Flame thickness and density ratio versus equivalence ratio.

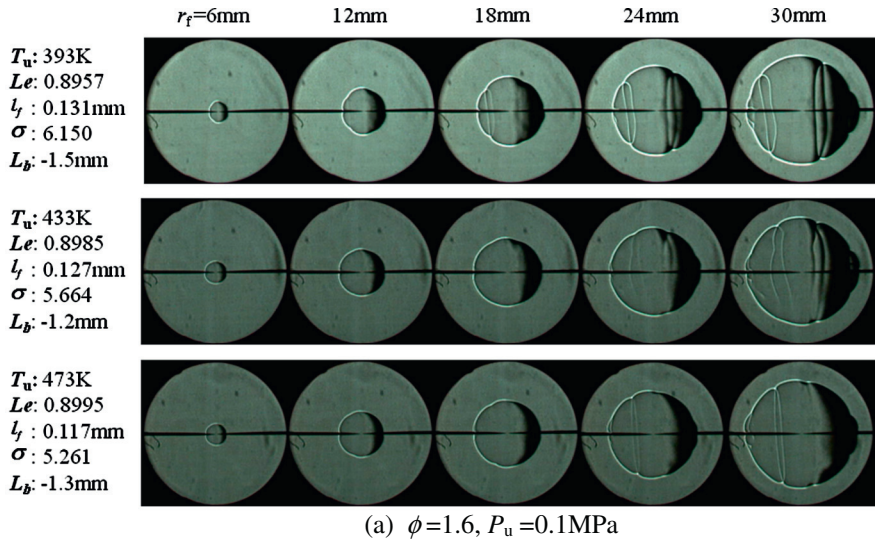

(a) ϕ=1.6, P_u =0.1MPa

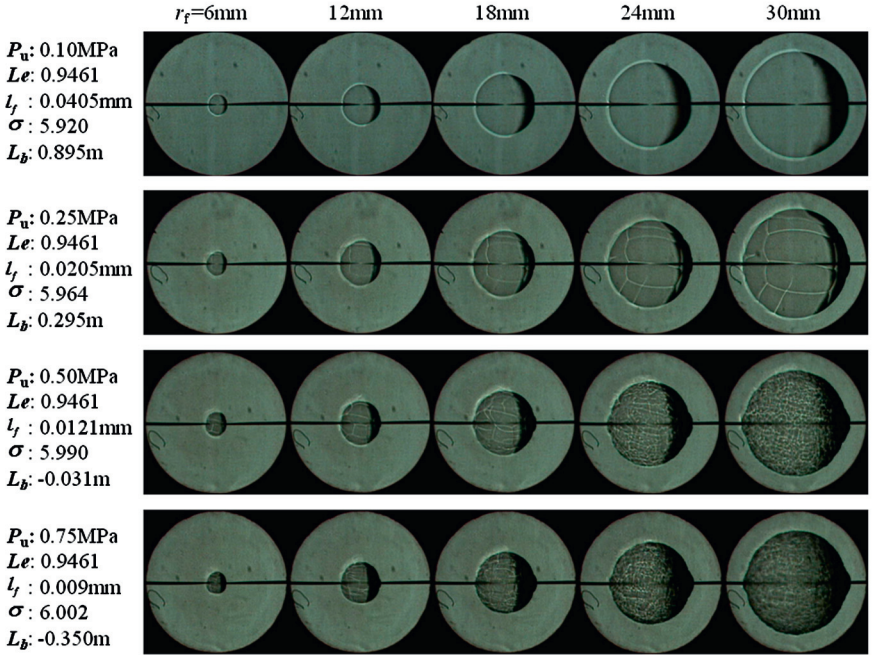

(b) ϕ=1.1, T_u =433K

Fig. 11. Schlieren photos of 2-methyl-1-butanol–air mixtures.

temperatures and pressures are given in Fig. 10. Lewis number shows a slight increase with the increase of temperature and this indicates a slight enhancement of the thermal-diffusivity instability. Density ratio decreases but no significant change on flame thickness with the increase of temperature suggests that the hydrodynamic instability is still weak. Combined effect of the two instabilities is characterized by the Markstein length, L_b, which shows insensitivity to temperature. As pressure is increased, Lewis number maintains unchanged, flame thickness is decreased and density ratio is slightly increased, leading to the enhancement of flame instability. This is consistent to the variation of Markstein length as shown in Fig. 9b.

Fig. 11a shows the schlieren photos of 2-methyl-1-butanol–air mixture at ϕ = 1.6, P_u = 0.1 MPa and three elevated temperatures. Flame instability characterized parameters, Lewis number, flame thickness, density ratio and Markstein length, are listed at the left side of the photos. Flame front shows the similar morphology with the increase of temperature. In the early stage, flame propagates with a smooth front surface. Cracks on flame front surface appear and develop as flame develops. The effect of flame stretch and thermo-diffusion causes the instability of flame front and makes the cracks on the flame front surface. Fig. 11b gives the images of the spherically expanding flame of 2-methyl-1-butanol–air mixture at ϕ = 1.1, T_u = 433 K and four pressures. At pressure of 0.1 MPa, flame front maintains a smooth surface during flame propagation. When pressure is elevated to 0.25 MPa, cracks on the flame front surface appear as flame develops. The cracks are from the perturbations generated by electrodes and spark energy. Flame still maintains stabilized without further development of cracks. As pressure is elevated to 0.5 MPa or 0.75 MPa, due to a strong curvature-induced stretch, flame front surface is wrinkled or even develops into the cellular structure, reflecting a strong instable flame front. The results are in consistent to variation of the Markstein length as pressure is increased.

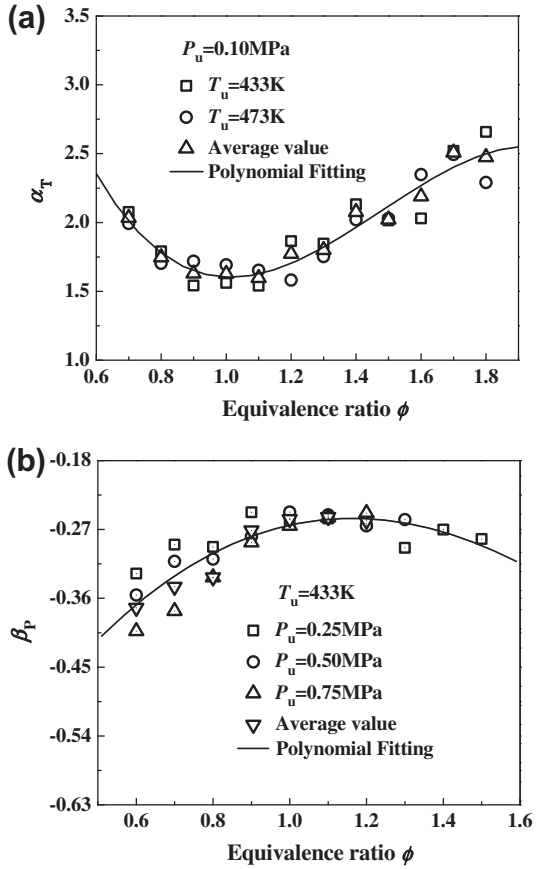

Fig. 12. Temperature and pressure exponents.

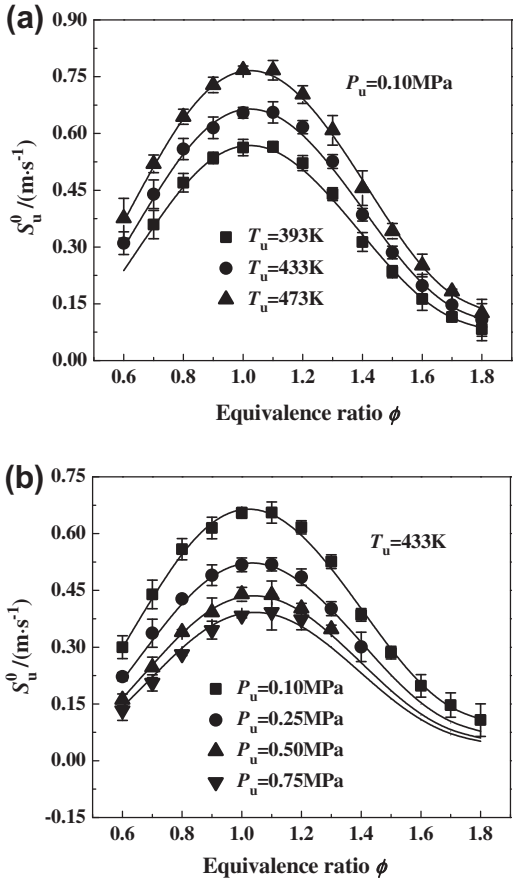

Fig. 13. Calculation of laminar flame speeds with correlation at different initial temperatures and pressures.

3.4. Normalization and empirical correlation

Laminar flame speed increases with the increase of temperature and decreases with the increase of pressure. It exhibits a non-monotonic variation to the equivalence ratio. A correlation between laminar flame speed and initial temperature as well as pressure is taken the form of,

$$S_u^0 = S_u^0(\phi)\left(\frac{T_u}{T_{u0}}\right)^{\alpha_T(\phi)}\left(\frac{P_u}{P_{u0}}\right)^{\beta_P(\phi)} \quad (7)$$

where the subscript 0 refers to the reference condition, $S_u^0(\phi)$, $\alpha_T(\phi)$, $\beta_P(\phi)$ are the laminar flame speed at the reference condition, temperature exponent, and pressure exponent, respectively. To decouple the nonlinear temperature and pressure dependency of the 2-methyl-1-butanol–air mixture, the correlation at reference condition is fitted. At pressure of 0.1 MPa and temperature of 393 K, the laminar flame speed is fitted as,

$$S_u^0(\phi) = 2.90025 - 16.61731\phi + 35.19509\phi^2 - 31.86315\phi^3 + 12.88419\phi^4 - 1.92435\phi^5 \quad (8)$$

When pressure is constant, Eq. (7) is simplified to,

$$S_u^0 = S_u^0(\phi)\left(\frac{T_u}{T_{u0}}\right)^{\alpha_T(\phi)} \quad (9)$$

The temperature exponent is,

$$\alpha_T(\phi) = \ln\left(\frac{S_u^0}{S_u^0(\phi)}\right) \Big/ \ln\left(\frac{T_u}{T_{u0}}\right) \quad (10)$$

The values of $\alpha_T(\phi)$ at different initial temperatures are given in Fig. 12a. The temperature exponent varies little to the variation of temperature. The temperature exponent is fitted as a function of equivalence ratio,

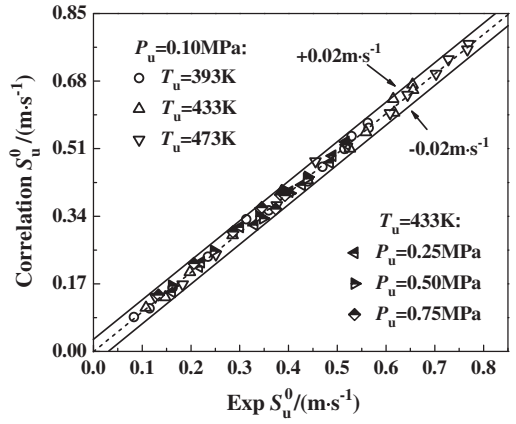

Fig. 14. Parity plot between experimental data and correlation predictions.

$$\alpha_T(\phi) = 7.61466 - 14.37684\phi + 10.80882\phi^2 - 2.44461\phi^3 \quad (11)$$

Similarly, the pressure exponent in Fig. 10b is fitted as a function of equivalence ratio,

$$\beta_P(\phi) = -0.77936 + 0.97034\phi - 0.50623\phi^2 + 0.0509\phi^3 \quad (12)$$

A correlation was obtained for the 2-methyl-1-butanol–air mixture,

$$S_u^0 = S_u^0(\phi)(T_u/393)^{\alpha_T(\phi)}(P_u/0.1)^{\beta_T(\phi)} \quad (13)$$

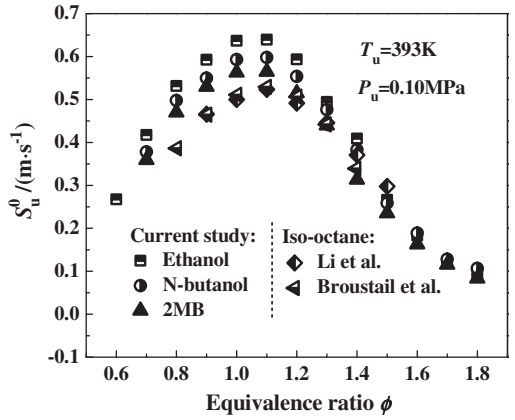

Fig. 15. Laminar flame speeds of ethanol, n-butanol, 2-methyl-1-butanol and iso-octane at P_u = 0.1 MPa and T_u = 393 K.

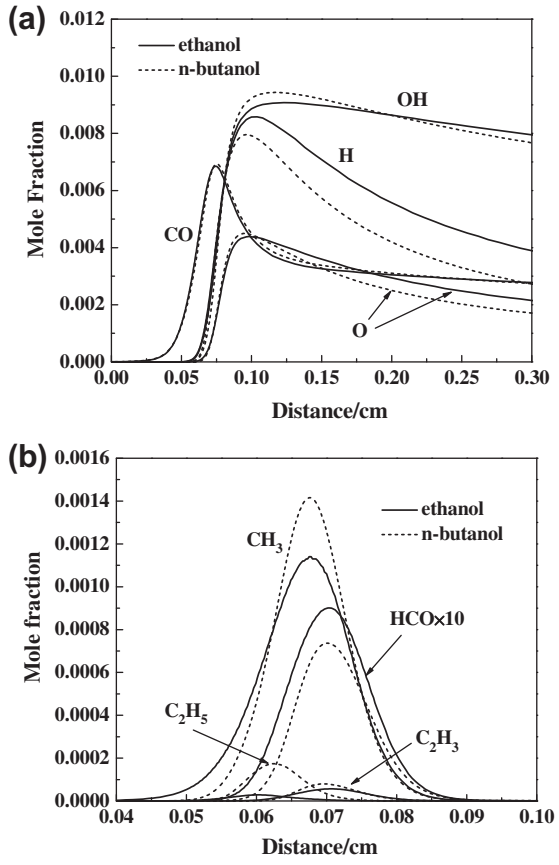

Fig. 16. Species mole fractions at $\phi = 1.0$, P_u = 0.1 MPa and T_u = 393 K.

Fig. 13 gives the comparison of laminar flame speeds between the calculated and measured values. The correlation can accurately calculate the laminar flame speeds at all equivalence ratios, temperatures and pressures. Parity plot between correlation calculation and experimental data is given in Fig. 14. The deviation of prediction on laminar flame speeds is within ±0.02 m/s^2.

3.5. Comparison among different fuels

Ethanol and butanol are the most concerned bio-alcohol fuels during the past decade. A comparison of 2-methyl-1-butanol with ethanol and butanol can provide an intuitive understanding of these fuels. Fig. 15 gives the comparison of the measured laminar flame speeds of ethanol, butanol, 2-methyl-1-butanol with those of iso-octane [18,39]. For the lean and stoichiometric mixtures, the laminar flame speeds of ethanol give higher values than those of n-butanol. From the comparison of some key radicals in the ethanol and n-butanol flames in Fig. 16, it can be seen that the chain branching radical, H, in the ethanol flame is significantly higher than that in the n-butanol flame, while key specie in the chain termination reactions, CH_3, is lower than that in the n-butanol flame, and this can explain the higher value of ethanol. Laminar flame speed of 2-methyl-1-butanol gives the slightly lower value than that of n-butanol, and higher value than that of iso-octane. So far, a detailed chemistry mechanism of 2MB is unavailable, so we can't analyze the difference between the fuels in kinetics. However, 2-methyl-1-butanol is the structure with a methyl attaching to the inner carbon atom (–CH_2) of n-butanol. Thus, 2-methyl-1-butanol has two methyl groups, while n-butanol has one methyl group. More methyl groups possess higher energy barrier for the H abstraction and lead to a slow reaction rate [20]. Iso-octane possesses the most methyl groups, and gives the lowest value. It also noted that the laminar flame speeds of these fuels are very close for the rich mixtures.

4. Conclusions

Measurements of laminar flame speeds and analysis on flame instability were made for 2-methyl-1-butanol–air mixtures at temperatures of 393, 433 and 473 K, pressures of 0.1, 0.25, 0.5 and 0.75 MPa, and equivalence ratios from 0.6 to 1.8. The main conclusions are as follows:

(1) Laminar flame speeds of 2-methyl-1-butanol–air mixtures were measured at different pressures and temperatures. For the 2-methyl-1-butanol–air mixture, laminar flame speed and mass burning flux increase with the increase of temperature. Laminar flame speed decreases and mass burning flux increases with the increase of pressure.
(2) Flame instability is insensitive to temperature but is enhanced with the increase of pressure.
(3) A correlation of laminar flame speed of 2-methyl-1-butanol–air mixture was given as function of equivalence ratio, pressure and temperature on the basis of experimental data.
(4) Laminar flame speeds of 2-methyl-1-butanol are close to those of n-butanol, but they are lower than those of ethanol and higher than those of iso-octane. Fuels give close values of laminar flame speeds at rich mixture side among ethanol, *n*-butanol, 2-methyl-1-butanol and iso-octane.

Acknowledgments

This work is supported by National Natural Science Foundation of China (51136005, 50876085) and National Basic Research Program (2013CB228406).

Appendix A. Supplementary material

Supplementary data of laminar flame speeds associated with this article can be found, in the online version, at http://dx.doi.org/10.1016/j.fuel.2013.05.039.

References

[1] Mascal M, Nikitin EB. Direct high-yield conversion of cellulose into biofuel. Angew Chem Int Ed 2008;47:7924–6.

[2] Black G, Curran HJ, Pichon S, Simmie JM, Zhukov V. Bio-butanol: combustion properties and detailed chemical kinetic model. Combust Flame 2010;157:363–73.
[3] Dernotte J, Mounaim-Rousselle C, Halter F, Seers P. Evaluation of butanol–gasoline blends in a port fuel-injection, spark-ignition engine. Oil Gas Sci Technol 2010;65:345–51.
[4] Jin C, Yao MF, Liu HF, Lee CF, Ji J. Progress in the production and application of n-butanol as a biofuel. Renew Sust Energy Rev 2011;15:4080–106.
[5] Szwaja S, Naber JD. Combustion of *n*-butanol in a spark-ignition IC engine. Fuel 2010;89:1573–82.
[6] Zhao L, Ye LL, Zhang F, Zhang LD. Thermal decomposition of 1-pentanol and its isomers: A theoretical study. J Phys Chem A 2012;116:9238–44.
[7] Cann AF, Liao JC. Pentanol isomers synthesis in engineered microorganisms. Appl Microbiol Biotechnol 2010;85:893–9.
[8] Cann AF. BIOT 80-Production of 2-methyl-1-butanol in engineered Escherichia coli. Abstracts of Papers of the American Chemical Society; 2009.
[9] Cann AF, Liao JC. Production of 2-methyl-1-butanol in engineered Escherichia coli. Appl Microbiol Biotechnol 2008;81:89–98.
[10] Shen CR, Liao JC. Photosynthetic production of 2-methyl-1-butanol from CO_2 in cyanobacterium Synechococcus elongatus PCC7942 and characterization of the native acetohydroxyacid synthase. Energy Environ Sci 2012;5(11):9574–83.
[11] Metghalchi M, Keck JC. Burning velocities of mixtures of air with methanol, isooctane, and indolene at high-pressure and temperature. Combust Flame 1982;48:191–210.
[12] Saeed K, Stone CR. Measurements of the laminar burning velocity for mixtures of methanol and air from a constant-volume vessel using a multizone model. Combust Flame 2004;139:152–66.
[13] Liao SY, Jiang DM, Huang ZH, Zeng K. Characterization of laminar premixed methanol–air flames. Fuel 2006;85:1346–53.
[14] Zhang ZY, Huang ZH, Wang XG, Xiang J, Wang XB, Miao HY. Measurements of laminar burning velocities and Markstein lengths for methanol–air–nitrogen mixtures at elevated pressures and temperatures. Combust Flame 2008;155(3):358–68.
[15] Gulder OL. Burning velocities of ethanol isooctane blends. Combust Flame 1984;56:261–8.
[16] Liao SY, Jiang DM, Huang ZH, Zeng K, Cheng Q. Determination of the laminar burning velocities for mixtures of ethanol and air at elevated temperatures. Appl Therm Eng 2007;27:374–80.
[17] Marinov NM. A detailed chemical kinetic model for high temperature ethanol oxidation. Int J Chem Kinet 1999;31:183–220.
[18] Broustail G, Seers P, Halter F, Moréac G, Mounaim-Rousselle C. Experimental determination of laminar burning velocity for butanol and ethanol iso-octane blends. Fuel 2011;90:1–6.
[19] Veloo PS, Egolfopoulos FN. Flame propagation of butanol isomers/air mixtures. Proc Combust Inst 2011;33:987–93.
[20] Gu XL, Huang ZH, Wu S, Li QQ. Laminar burning velocities and flame instabilities of butanol isomers–air mixtures. Combust Flame 2010;157:2318–25.
[21] Tsujimura T, Pitz WJ, Gillespie F, Curran HJ, Weber BW, Zhang Y, et al. Development of isopentanol reaction mechanism reproducing autoignition character at high and low temperatures. Energy Fuels 2012;26:4871–86.
[22] Heufer KA, Sarathy SM, Curran HJ, Davis AC, Westbrook CK, Pitz WJ. Detailed kinetic modeling study of n-pentanol oxidation. Energy Fuels 2012;26:6678–85.
[23] Togbe C, Halter F, Foucher F, Mounaim-Rousselle C, Dagaut P. Experimental and detailed kinetic modeling study of 1-pentanol oxidation in a JSR and combustion in a bomb. Proc Combust Inst 2011;33:367–74.
[24] Dayma G, Togbe C, Dagaut P. Experimental and detailed kinetic modeling study of isoamyl alcohol (isopentanol) oxidation in a jet-stirred reactor at elevated pressure. Energy Fuels 2011;25:4986–98.
[25] Tang CL, Wei LJ, Man XJ, Zhang JX, Huang ZH, Law CK. High temperature ignition delay times of C5 primary alcohols. Combust Flame 2013;160:520–9.
[26] Gu XL, Huang ZH, ; Li QQ, Tang CL. Measurements of laminar burning velocities and Markstein lengths of n-butanol–air premixed mixtures at elevated temperatures and pressures. Energy Fuels 2009;23:4900–7.
[27] Tang CL, Huang ZH, Zheng JJ, Wang JH. Study on nitrogen diluted propane–air premixed flames at elevated pressures and temperatures. Energy Convers Manage 2010;51:288–95.
[28] Tang CL, He JJ, Huang ZH, Jin C, Wang JH, Wang XB, et al. Measurements of laminar burning velocities and Markstein lengths of propane–hydrogen–air mixtures at elevated pressures and temperatures. Int J Hydrogen Energy 2008;33:7274–85.
[29] Zhang X, Huang ZH, Zhang ZY, Zheng JJ, Yu W, Jiang DM. Measurements of laminar burning velocities and flame stability analysis for dissociated methanol–air–diluent mixtures at elevated temperatures and pressures. Int J Hydrogen Energy 2009;34:4862–75.
[30] Sarathy SM, Thomson MJ, Togbé C, Dagaut P, Halter F, Mounaim-Rousselle C. An experimental and kinetic modeling study of n-butanol combustion. Combust Flame 2009;152:852–64.
[31] Wu XS, Huang ZH, Jin C, Wang XG, Wei LX. Laminar burning velocities and Markstein lengths of 2,5-dimethylfuran–air premixed flames at elevated temperatures. Combust Sci Technol 2011;183:220–37.
[32] Bradley D, Gaskell PH, Gu XJ. Burning velocities, Markstein lengths, and flame quenching for spherical methane–air flames: a computational study. Combust Flame 1996;104:176–98.
[33] Gu XL, Li QQ, Huang ZH. Laminar burning characteristics of diluted n-butanol/air mixtures. Combust Sci Technol 2011;183:1360–75.
[34] Tang CL, Huang ZH, Jin C, He JJ, Wang JH, Wang XB, et al. Measurements of laminar burning velocities and Markstein lengths of propane–hydrogen–air mixtures at elevated pressures and temperatures. Int J Hydrogen Energy 2008;33:7274–85.
[35] Wu XS, Huang ZH, Jin C, Wang XG, Zheng B, Zhang YJ, et al. Measurements of laminar burning velocities and Markstein lengths of 2,5-dimethylfuran–air–diluent premixed flames. Energy Fuels 2009;23:4355–62.
[36] Law CK, Sung CJ. Structure, aerodynamics, and geometry of premixed flamelets. Prog Energy Combust Sci 2000;26:459–505.
[37] Gu XJ, Haq MZ, Lawes M, Woolley R. Laminar burning velocity and Markstein lengths of methane–air mixtures. Combust Flame 2000;121:41–58.
[38] Qin X, Ju YG. Measurements of burning velocities of dimethyl ether and air premixed flames at elevated pressures. Proc Combust Inst 2005;30:233–40.
[39] Li QQ, Hu EJ, Zhang XY, Cheng Y, Huang ZH. Laminar flame speeds and flame instabilities of pentanol isomer–air mixtures at elevated temperatures and pressures. Energy Fuels 2013;27:1141–50.
[40] Bradley D, Sheppart CGW, Woolley R, Greenhalgh DA, Lockett RD. The development and structure of flame instabilities and cellularity at low Markstein numbers in explosions. Combust Flame 2000;122:195–209.
[41] Law CK, Jomaas G, Bechtold JK. Cellular instabilities of expanding hydrogen/propane spherical flames at elevated pressures: theory and experiment. Proc Combust Inst 2005;30:159–67.
[42] Landau L. On the theory of slow combustion. Acta Physicochim URSS 1944;19:77–85.
[43] Darrieus G. Propagation d'un front de flame. Proceedings of La Technique Moderne et le Congrès de Méchanique Appliquée; Paris, France; 1938.
[44] Bechtold JK, Matalon M. Hydrodanamic and diffusion effects on the stability of spherically expanding flames. Combust Flame 1987;67:77–90.